Determination of the Integrated Luminosity at HERA using Elastic QED Compton Events

Stefan Schmitt on behalf of the H1 Collaboration

DESY, Notkestraße 85, 22607 Hamburg, Germany, sschmitt@mail.desy.de

DOI: `http://dx.doi.org/10.3204/DESY-PROC-2012-02/109`

A measurement of the integrated luminosity at the ep collider HERA is presented, exploiting the elastic QED Compton process $ep \to e\gamma p$. The electron and the photon are detected in the backward calorimeter of the H1 experiment. The integrated luminosity of the data recorded in 2003 to 2007 is determined with a precision of 2.3%. The measurement is found to be compatible with the corresponding result obtained using the Bethe-Heitler process.

1 Introduction

For particle collider experiments, the precise knowledge of the integrated luminosity is essential for any type of cross section measurement. The time-integrated luminosity is often determined from the event count N observed in a process with well-known cross section σ as $\mathcal{L} = N/\sigma$. At the ep collider HERA, electrons[1] and protons were colliding head-on at energies $E_e^0 = 27.5\,\mathrm{GeV}$ and $E_p^0 = 920\,\mathrm{GeV}$, respectively. The reaction used to determine the integrated luminosity is the production of a radiative photon in elastic ep scattering, $ep \to e\gamma p$. Depending on the phase space considered, this process is referred to as Bethe-Heitler (BH) scattering or QED Compton (QEDC) scattering. In the BH process [1] both the electron and the photon are emitted almost collinearly to the incident electron. The corresponding cross section is very large, $\mathcal{O}(100\,\mathrm{mb})$. For QEDC scattering [2] the particles have a sizable transverse momentum with respect to the incident electron and can be detected in the main detector. The momentum transfer squared at the proton vertex, t, is generally small. At very small momentum transfer $|t| \ll 1\,\mathrm{GeV}^2$, elastic scattering dominates. At $|t| \gtrsim 1\,\mathrm{GeV}^2$, inelastic processes are relevant and the reaction is sensitive to the proton structure. In addition, there are quasi-elastic contributions to the cross section, where the outgoing proton forms an excited state, like Δ or $N^\star$, which then decays to a low mass hadronic system. Within the phase space considered in this analysis, the elastic QEDC cross section is $\mathcal{O}(50\,\mathrm{pb})$. The Compton process, including quasi-elastic and inelastic contributions, is simulated using the COMPTON22 event generator [3].

At HERA, the integrated luminosity is usually measured in the BH process, using dedicated detectors located at small angles. The advantage of this process is its very large cross section, thus negligible statistical uncertainties are achieved for small amounts of integrated luminosity. However, there are various sources of possibly large systematic uncertainty, like acceptance limitations for the small angle detectors and details of the HERA beam optics.

[1] The term "electron" is used generically to refer to both electrons and positrons.

Here, a determination of the integrated luminosity is presented, based on the elastic QEDC process, which is measured in the H1 main detector [4]. Both the scattered electron and photon are detected in the H1 rear calorimeter (SpaCal) [5]. The position of the interaction vertex along the beam direction is determined using the central inner proportional chambers (CIP) [6]. This method is insensitive to details of the beam optics. However, the smallness of the cross section leads to limited statistical precision.

2 Event selection

Elastic QEDC events are selected by requiring two clusters in the electromagnetic section of the SpaCal. The transverse sizes of the SpaCal clusters are restricted to $R_{\log} < 6\,\text{cm}$, where $R_{\log}$ is calculated from the SpaCal cell centres using logarithmic energy weighting [7]. The cluster energies are required to be larger than 2.2 GeV. In the range $30 \leq R < 72\,\text{cm}$ of the radial distance from the beam, R, exactly two such clusters are required, whereas for $20 \leq R < 30\,\text{cm}$ no cluster is allowed. The restriction $R \geq 30\,\text{cm}$ on the two clusters ensures that the particles are within the CIP acceptance. Electron trajectories and the position of the vertex are reconstructed using the SpaCal cluster position together with position information from the CIP chambers. If there is only one SpaCal cluster with CIP hits, that cluster is taken as electron while the other cluster is taken as photon. If both SpaCal clusters have CIP hits, it is assumed that the photon has converted into an electron-positron pair while passing the material in front of the CIP detector and the particle assignment is done according to the hypothesis yielding an azimuthal opening angle of the two particles closest to 180°. Only events with longitudinal vertex position $|z_{\text{vtx}}| < 35\,\text{cm}$ are selected in the analysis. In addition, the following cuts are applied: energy of the most (least) energetic particle greater than 10 (7) GeV, polar angles θ_e, θ_γ within 155.9° and 169.5°, difference in azimuth between 170° and 190°. Inelastic background sources are further suppressed by using conditions on additional activity in the detector, such as limited energy in the forward part of the LAr calorimeter, and a veto on the number of tracks in the central tracking detectors. Finally, the modulus of the transverse component of the missing momentum, P_T^{miss}, is used as the main discriminating variable. Figure 1 shows the composition of the event sample differential in the variable P_T^{miss}, where the signal and various background processes are indicated. The elastic QEDC process dominates at small P_T^{miss}. At high P_T^{miss}, quasi-elastic and inelastic QEDC processes are dominant. Other background sources include electron-positron pair production, $ep \to ep\,e^-e^+$, simulated with GRAPE [8] and various diffractive processes like deeply virtual Compton scattering, modelled with MILOU [9], diffractive vector meson production, simulated with DIFFVM [10] and non-resonant diffrac-

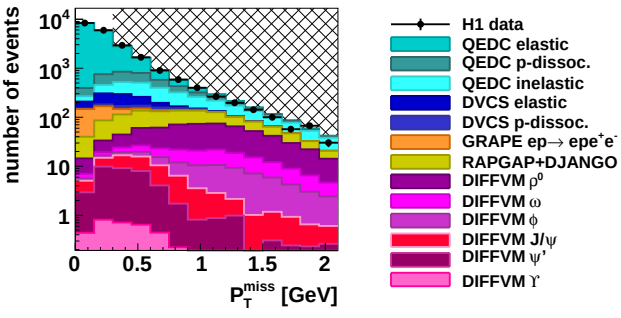

Figure 1: distribution of the missing transverse momentum. The data are shown as black dots. The total prediction and contributions from various background sources are indicated. The region $P_T^{\text{miss}} > 0.3\,\text{GeV}$ is excluded.

tion, modelled with RAPGAP [11].
A selection criterion $P_T^{\text{miss}} < 0.3\,\text{GeV}$ is applied. Within the selected region 14277 candidate events are observed and the fraction of background amounts to 8%.

3 Systematic uncertainties

Table 1 summarises the contributions to the uncertainties of the luminosity measurement. Systematic effects dominate over statistical uncertainties. The contributions to the uncertainty from experimental conditions, background normalisation and QEDC theory are similar in size.

Experimental uncertainties	**1.4%**
Background uncertainties	**1.2%**
QEDC theory uncertainties	**1.1%**
Statistical uncertainty	**0.8%**
Total uncertainty	**2.3%**

Table 1: Summary of the uncertainties on the determination of the integrated luminosity using elastic QEDC events.

The experimental uncertainties are dominated by the SpaCal energy resolution. The energy resolution is monitored using the double-angle reconstruction method [12] for the transverse momentum, P_T^{DA}. Distributions of the ratio of measured transverse momentum over P_T^{DA} are used to calibrate the energy resolution in the simulation. The calibration is repeated for electrons, non-coverted photons and converted photons, respectively.

The background uncertainties are dominated by the normalisation of the quasi-elastic and inelastic QEDC contributions. These are monitored using fits to the distribution of the components of the total transverse momentum parallel and perpendicular to the electron transverse momentum. The fits are performed outside the signal region, for $P_T^{\text{miss}} > 0.3\,\text{GeV}$

The uncertainties to the elastic QEDC theory are dominated by higher order effects. Initial state radiation is modelled as described in [13] using a photon radiator [14]. As an alternative the peaking approximation [15] as implemented in the COMPTON22 generator is considered. The difference between these models dominates the theory uncertainty.

The distribution of $\sum(E - p_z)/(2E_e^0)$, calculated from the sum of the electron and photon four-momenta, is shown in figure 2. This variable estimates the momentum fraction of the electron entering the hard collision after initial state radiation. The systematic uncertainties are shown differential in $\sum(E - p_z)/(2E_e^0)$. The width of the peak near 1 is dominated by energy resolution effects. The tail towards lower $\sum(E - p_z)/(2E_e^0)$ is sensitive to initial state radiation and to background processes. The simulation is capable to describe the data within uncertainties.

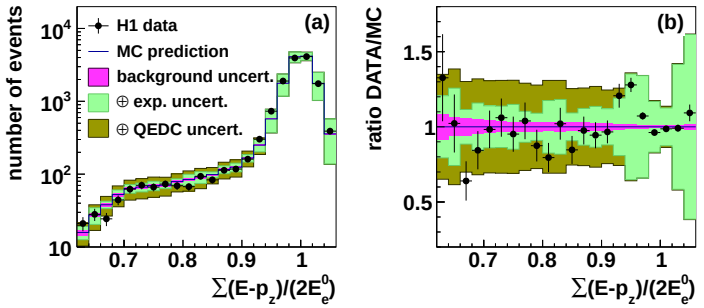

Figure 2: distribution of the variable $\sum \frac{E-p_z}{2E_e^0}$. The data are shown as black dots. The total prediction and contributions from various sources of systematic uncertainty are indicated.

4 Results

The integrated luminosity of the H1 data collected in the years 2003 to 2007 is determined using elastic QED Compton events. For the data sample as used in this paper, an integrated luminosity of $\mathcal{L}^{\mathrm{QEDC}} = 351.6 \pm 8.0\,\mathrm{pb}^{-1}$ is measured. The statistical uncertainty amounts to 0.8%, whereas the total systematic error is 2.1%. The integrated luminosity is in agreement with the Bethe-Heitler measurement, $\mathcal{L}^{\mathrm{BH}} = 338.9 \pm 10.2\,\mathrm{pb}^{-1}$.

References

[1] H. Bethe and W. Heitler, Proc. Roy. Soc. Lond. **A146** (1934) 83.

[2] W. Beenakker, F. A. Berends and W. L. van Neerven, Proc. of Workshop on Radiative Corrections for e^+e^- collisions, ed. J. H. Kühn, Ringberg Castle, Tegernsee (1989); J. Blümlein, Z. Phys. **C47** (1990) 89;

J. Blumlein, G. Levman and H. Spiesberger, J. Phys. **G19** (1993) 1695;

J. Blumlein, Z. Phys. **C65** (1995) 293 [hep-ph/9403342].

[3] A. Courau and P. Kessler, Phys. Rev. **D46** (1992) 117;
V. Lendermann, H. C. Schultz-Coulon and D. Wegener, Eur. Phys. J. **C31** (2003) 343 [hep-ph/0307116].

[4] I. Abt *et al.* [H1 Collaboration], Nucl. Instrum. Meth. **A386** (1997) 310;
I. Abt *et al.* [H1 Collaboration], Nucl. Instrum. Meth. **A386** (1997) 348.

[5] R. Appuhn *et al.* [H1 SpaCal Group], Nucl. Instrum. Meth. **A386** (1997) 397.

[6] J. Becker *et al.*, Nucl. Instrum. Meth. **A586** (2008) 190 [physics/0701002].

[7] A. Glazov, N. Raicevic and A. Zhokin, Comput. Phys. Commun. **181** (2010) 1008.

[8] T. Abe, GRAPE-Dilepton version 1.1, Comput. Phys. Commun. **136** (2001) 126 [hep-ph/0012029].

[9] E. Perez, L. Schoeffel and L. Favart, hep-ph/0411389.

[10] B. List, A. Mastroberardino, Proc. of the Workshop on Monte Carlo Generators for HERA Physics, eds. A. Doyle *et al.*, DESY-PROC-1999-02 (1999) 396.

[11] RAPGAP 3.1: H. Jung, Comput. Phys. Commun. **86** (1995) 147.

[12] S. Bentvelsen, J. Engelen and P. Kooijman, Proc. of the Workshop on Physics at HERA, eds. W. Buchmüller, G. Ingelman, Hamburg, DESY (1992) 23;

K. C. Hoeger, *ibid.* 43.

[13] H. Anlauf *et. al* [Darmstadt-Siegen Collaboration], Z. Phys. **C52** (1991) 655.

[14] G. Montagna, O. Nicrosini and L. Trentadue, Nucl. Phys. **B357** (1991) 390.

[15] E. Etim, G. Pancheri and B. Touschek, Nuovo Cim. **B51** (1967) 276;
G. Pancheri, Nuovo Cim. **A60** (1969) 321.